Int. J. Electrochem. Sci., 14 **(2019)** 743 – 754, doi: 10.20964/2019.01.39

International Journal of
ELECTROCHEMICAL
SCIENCE
www.electrochemsci.org

Facile One-pot Synthesis of Carbon Supported PdCuCo Nanoalloy Catalysts for Formic Acid Electrooxidation

Yumeng Ma[1], *Yunhua Li*[1], *Pengwei Li*[1], *Qiaoxia Li*[1,2,*]

[1] Shanghai Key Laboratory of Materials Protection and Advanced Materials in Electric Power, College of Environmental and Chemical Engineering, Shanghai University of Electric Power, 2588 Changyang Road, Yangpu District, Shanghai 200090, China
[2] Shanghai institute of pollution control and ecological security, Shanghai 200090, P. R. China
[*]E-mail: liqiaoxia@shiep.edu.cn

Received: 20 September 2018 / *Accepted:* 1 November 2018 / *Published:* 30 November 2018

PdCuCo/C nanoalloy catalysts were prepared via a facile one-pot liquid phase chemical reduction. Ethylene glycol was used as the reducing agent and reaction media, trisodium citrate as the stabilizer, and acid-pretreated Vulcan XC-72R carbon powder as the carrier material. The morphology, structure, and electrochemical performances of the as-prepared PdCuCo/C nanoalloy catalysts were characterized and analyzed. The PdCuCo alloy nanoparticles are uniformly dispersed on the carbon surface with a smaller particle size than that of Pd/C. The PdCuCo/C catalysts showed higher catalytic activity and stability for the oxidation of formic acid compared with the Pd/C catalyst prepared via the same method. The oxidation peak current density of PdCuCo/C reaches 60.0 mA cm^{-2}, which is 1.8 times that of the Pd/C. The chronoamperometry curves reveal that the current density of PdCuCo/C catalyst is 6.7 times that of the Pd/C catalyst after 3600 s. The electrochemically active surface area (ESCA) of the PdCuCo/C catalysts (99.5 $m^2 \cdot g^{-1}$) is much higher than that of the Pd/C (55.7 $m^2 \cdot g^{-1}$). These results indicate that the PdCuCo/C nanoalloy catalysts show great potential as anode electrocatalysts in direct formic acid fuel cells (DFAFCs).

Keywords: PdCuCo/C; Nanoalloy; Electrocatalyst; Formic acid oxidation

1. INTRODUCTION

The energy crisis and environmental issues have become severe. However, fuel cells have attracted widespread attention due to their high efficiency and cleanliness. Among many fuel cells, the direct formic acid fuel cell (DFAFC) is non-toxic, offers a high open circuit potential, safe transportation and storage, and low permeability to Nafion membrane [1-3]. Compared with hydrogen storage polymer

electrolyte membrane fuel cells and direct methanol fuel cells, DFAFC exhibits both a higher electromotive force and energy density, and is also becoming a promising portable energy device [4].

Currently, Pt-based catalysts [5-6] are commonly the anode catalysts used in fuel cells; however, Pt resources are scarce, expensive, and susceptible to CO poisoning, which limits their application in fuel cells. Several studies have shown that Pd-based catalysts achieve better formic acid electrocatalytic oxidation activity [7]. It has also been found that the electrochemical activity and stability of Pd-based bimetallic and trimetallic catalysts in fuel cell anode catalysts are superior to those of pure Pd catalysts [8-9]. Therefore, the addition of one or more transition metals to design carbon supported Pd/ transition-metal catalysts, such as Pd-Cu/C [10-15], Pd-Co/C [16-20], Pd-Au/C [21], Pd-Ag/C [22-23], and Pd-Ni/C [24-25], is an efficient strategy to reduce cost and promote catalytic activity at the same time. This is because transition metal alloying or surface modification is an important method of Pd-based catalyst modification [26-27]. Xia et al. [28] reported the synthesis of N-doped carbon black supported PdCu alloy nanocatalyst (PdCu/NCB) by a facile one-pot soft chemistry route. Douk A S and co-workers [29] fabricated a novel CuPd/C nanomaterial that exhibited exceptional activity for formic acid electrooxidation. In contrast to unitary or bimetallic catalysts [30−31], Pd-based trimetallic catalysts exhibit enhanced catalytic activity because of their adjusted electronic structure and surface atom rearrangement. For instance, Rostami H [32] developed a facile and clean electrochemical method for the preparation of ternary PdCuNi catalysts on the surface of carbon, and studied the effect of adding Ni on the electrocatalytic activity of ethanol electrooxidation of PdCu catalyst through experiments and theories and found the existing of Cu combined with Ni can improve the poison tolerance of Pd/C catalyst by removal of adsorbed CO-like intermediate species during ethanol oxidation. Zhang and colleagues [33] synthesized a superior ternary CuFePd electrocatalyst were anchored on reduced graphene oxide by one-pot chemical reduction. Further, Huang et al. [34] fabricated a novel PdCuBi/C catalyst that exhibited both a core-shell structure and surface modification towards ethylene glycol oxidation in an alkaline medium.

The addition of one or more transition metals may affect the performance of Pd-based catalysts for several reasons [35-36]: The outermost or second outer orbital electrons of the transition metal are in a full-empty, semi-full, and fully charged state, easily losing electrons or getting electrons. Therefore, electron transfer is likely to occur between Pd and the transition metal, and the state of the outer layer of Pd can be significantly changed after the alloy is formed. In addition, since the radius of the transition metal is smaller than the radius of Pd atom, the lattice parameter of Pd after alloying changes significantly, resulting in lattice distortion. Due to the existence of "electronic effect" and "lattice stress", the d-band center of Pd is lowered, and the Gibbs free energy required for electron transfer in the catalytic process is reduced. From the aspect of CO poisoning resistance ability, oxygen-containing groups can be provided under low potential conditions, which is favorable for the oxidation of toxic intermediate CO, and also changes the electronic structure of Pd and reduces the adsorption energy of CO on alloy catalysts.

In addition, Cu and Co have abundant reserves on the earth. The standard electrode potential of Cu^0/Cu^{2+} is 0.345 V, which indicates that Cu is more stable in acid-base electrolytes. After adding a little Cu and Co, the lattice constant of the precious metal can be changed to reduce the size of the metal particles and increase the specific surface area of the catalyst. At the same time, the d-band center of the

noble metal can be adjusted, the adsorption energy of the intermediate product can be reduced, and the adsorption of the poisoned product can be reduced. Therefore, PdCu/C and PdCo/C bimetallic catalysts exhibit good catalytic performance for formic acid [10-20].

On the basis of the above considerations, herein, a PdCuCo/C catalyst was synthesized with low-cost raw materials through a one-pot liquid-phase chemical reduction method. In the synthesis, ethylene glycol was used as both the reducing agent and the solvent. Compared with Pd/C, the PdCuCo/C nanoalloy catalyst exhibits e significantly higher catalytic activity and stability.

2. EXPERIMENTAL

2.1. Material

Ammonium tetrachloropalladate ($(NH_4)_2PdCl_4$), copper chloride dihydrate ($CuCl_2{\cdot}2H_2O$), cobalt nitrate hexahydrate ($Co(NO_3)_2{\cdot}6H_2O$), sodium citrate ($C_6H_5Na_3O_7{\cdot}2H_2O$), nitric acid ($HNO_3$), sulfuric acid ($H_2SO_4$), formic acid (HCOOH), ethanol (C_2H_5OH), ethylene glycol ($C_2H_6O_2$), hydrochloric acid (HCl), and sodium hydroxide (NaOH) were obtained from Sinopharm Chemical Reagent Co. Ltd. Vulcan XC-72R carbon was purchased from Cabot. Nafion solution (5 wt.%) was gotten from Dupont. All chemical reagents were analytical grade.

2.2. Synthesis of the catalyst

For preparing the PdCuCo/C catalyst, 26.7 mg $(NH_4)_2PdCl_4$, 16.0 mg $CuCl_2{\cdot}2H_2O$, 13.7 mg $Co(NO_3)_2{\cdot}6H_2O$ and 345.0 mg $C_6H_5Na_3O_7{\cdot}2H_2O$ were dissolved in 60 mL ethylene glycol and then placed in a three-necked bottle. The solution was stirred and 31.1 mg acid-pretreated Vulcan XC-72R carbon powder was added to the mixture. The mixture was stirred continuously for 12 h. Following this, 1 mol L^{-1} NaOH/EG solution was added to adjust the pH to 9. After stirring for 5 h under a nitrogen atmosphere at 160 °C, the mixture was cooled to 70 °C and 1 mol L^{-1} HCl was added to adjust the pH to 3. Following this, the mixture was stirred for another 2 h. After stirring, the solution was cooled to room temperature. Finally, the solution was washed with Milli-Q water and ethanol. The residue was dried at 60 °C for 12 h and then grounded in an agate mortar to get the carbon-supported PdCuCo nanoparticles (denotated as PdCuCo/C).

The carbon supported PdCu nanoparticles (denotated as PdCu/C, metallic loading of 20 wt%) and carbon supported Pd catalyst (denotated as Pd/C, metallic loading of 20 wt%) were also prepared in the same procedure.

2.3. Characterization

Transmission electron microscope (TEM) was conducted on a JEOL JEM-2100F with energy dispersive X-ray spectroscopy (EDS) analysis. X-ray diffraction (XRD) was carried out on a Bruker D8-ADVANCE with Cu Kα radiation (λ = 0.154 nm), where in the test angle ranged from 20° to 90°.

Inductively coupled plasma atomic emission spectra (ICP-AES) was performed using a HITACHI P-4010.

2.4. Electrochemical measurements

Electrochemical measurements were performed on CHI 660E electrochemistry workstations (CHENHUA Instrument, China) with conventional three-electrode system. A Pt wire and a saturated calomel electrode (SCE) were employed as counter and reference electrode, respectively. A glassy carbon electrode (GCE, diameter: 3 mm) was used as the working electrode. 5.6 μL catalyst ink containing 2 μg Pd was drop on the surface of GCE, and dried with infrared lamp. The cyclic voltammograms (CVs) were performed in 0.5 M H_2SO_4 with or without 0.5 M HCOOH at a scan rate of 50 mV s^{-1}. Chronoamperometry curves was conducted in 0.5 M H_2SO_4 with 0.5 M HCOOH at a scan rate of 50 mV s^{-1}. 30 min N_2 was passed through the solution before all tests to remove air in the solution. In addition, CO stripping measurements were collected in 0.5 M H_2SO_4 at a scan rate of 10 mV s^{-1}. The working electrode was immersed in the solution with bubbling CO for 15 min at -0.1 V (vs SCE). Then, the excess CO in the solution was removed by bubbling N_2 for 30 min. All electrochemical tests were performed at room temperature.

3. RESULTS AND DISCUSSION

3.1. Morphology characterization

The morphology and particle size distribution histograms of the Pd/C, PdCu/C, and PdCuCo/C catalysts are depicted in Figure 1. In Figure 1a, it can be seen that the Pd nanoparticle has no obvious agglomeration phenomenon for Pd/C with an average particle size of 5.3 nm, indicating that the Pd/C prepared by the ethylene glycol reduction method is worthy of study. PdCu alloy nanoparticles are found to possess better uniform dispersion with an average particle diameter of 4.7 nm compared with Pd/C. The TEM image of the PdCuCo/C catalyst indicates that the PdCuCo alloy nanoparticles are uniformly dispersed on the surface of the carbon black (Figure 1e) with an average particle size of approximately 4.3 nm and a size distribution of 2.5 nm to 7.0 nm (Figure 1f). The synthesized PdCuCo nanoparticles have a small and uniform size and are well dispersed on the carbon surface. Based on our results and analysis, the addition of Cu and Co elements will reduce the particle size of the catalyst and cause changes in the surface structure of the Pd, as well as the reaction between the surface-adsorbed species and the electronic effect contribute to the formic acid electrooxidation on the Pd nanoparticles. Therefore, the size effect could be one of the reasons leading to much higher catalytic activity of the PdCuCo/C catalysts for the formic acid electrooxidation than the Pd/C catalyst.

Figure 2(a) shows the XRD patterns of the Pd/C, PdCu/C, and PdCuCo/C catalysts. The broad peak at around 26° is indexed to the (002) plane of the acid-pretreated Vulcan XC-72R carbon, indicating that the catalyst has a high graphite structure and good electrical conductivity. The main peaks at 2θ values of 39.89°, 46.36°, 68.04°, 81.94°, and 86.71° correspond to the (111), (200), (220), (311) and

(222) crystal planes of face-centered cubic (fcc) Pd (PDF#46-1043). However, after adding Cu and Co to Pd/C, only the apparent fcc Pd (111) crystal plane was observed. In addition, the broadening of the (111) diffraction peak of Pd may be due to the smaller particle size of the synthesized catalyst, which is consistent with the conclusion obtained by TEM. The Pd (111) peak position of the PdCu/C and PdCuCo/C catalysts is shifted to a higher 2θ value compared to the same peak of the Pd/C catalysts, as shown in Figure 2(b), indicating that the lattice parameter shrinks because the Pd atoms were replaced by smaller Cu or Co. It is worthwhile noting that compared to PdCu/C, the Pd (111) peak of PdCuCo/C shifts to a lower degree. These results suggest that a ternary catalyst was successfully synthesized.

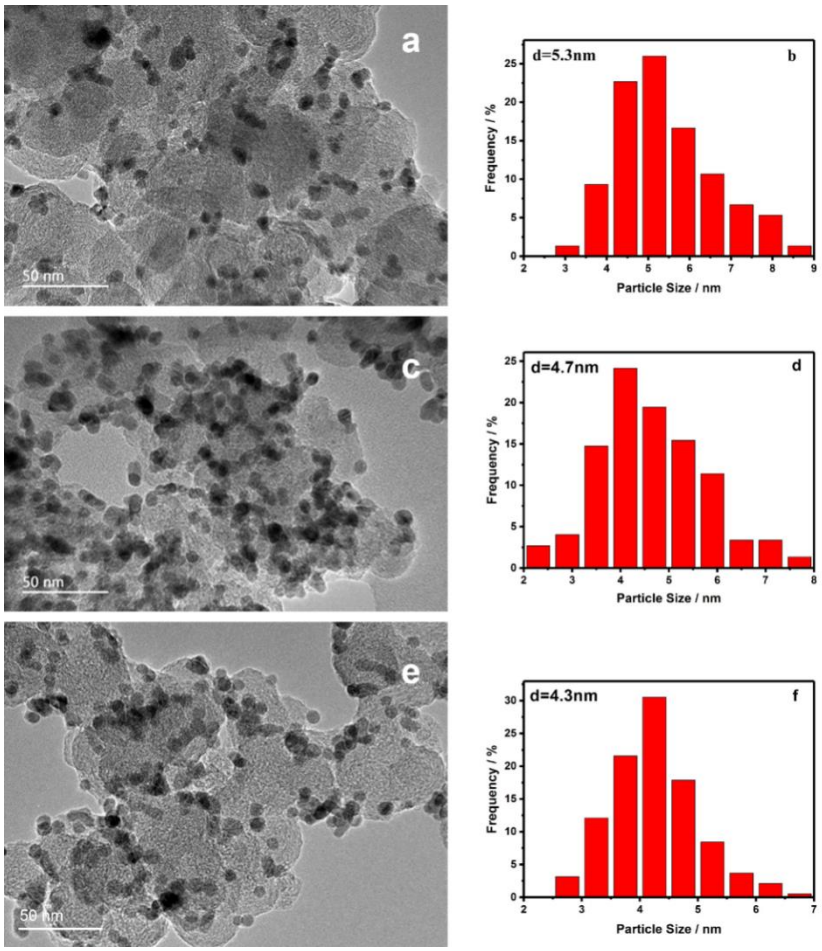

Figure 1. TEM images of Pd/C (a), PdCu/C (c), PdCuCo/C (e), and their particle size histograms of Pd/C (b), PdCu/C (d), PdCuCo/C (f).

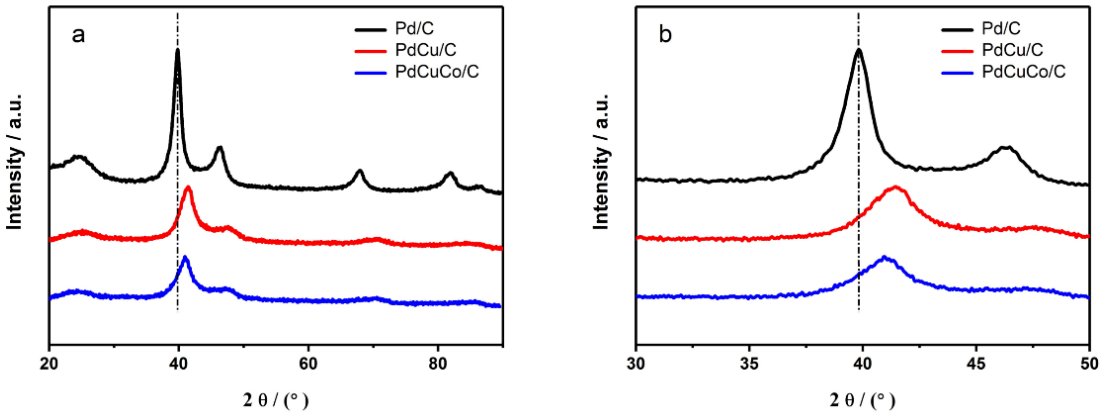

Figure 2. (a) XRD patterns of Pd/C, PdCu/C, PdCuCo/C catalysts. (b) XRD patterns located from 30° to 50° of Pd/C, PdCu/C, PdCuCo/C catalysts.

3.2. Electrochemical characterization

Figure 3 displays the cyclic voltammograms (CVs) for Pd/C (a), PdCu/C (b), and PdCuCo/C (c) in N_2-saturated 0.5 M H_2SO_4 at 50 mV s^{-1}. The peak appearing in the potential range of -0.20 ~ 0.08 V (vs. SCE) in the CVs curve is the hydrogen absorption / desorption peak of the catalysts. Due to the different crystal faces exposed by the precious metal, the absorption and desorption of hydrogen each contain two independent current peaks, which represent hydrogen oxidation desorption and hydrogen reductive adsorption reactions. It can be seen that the adsorption and desorption peaks of PdCu/C and PdCuCo/C are higher than those of Pd/C, suggesting that the addition of Cu and Co increases the hydrogen adsorption. From the CVs curve of the Pd/C catalyst, it can be found that Pd oxidation starting at -0.6 V (positive-going scan) and a reduction peak of Pd oxides at -0.5 V (negative-going scan) [37]. After adding Cu and Co, the metal oxide peak potentials of the two catalysts shift to negative values compared with Pd/C, indicating that the metal needs a higher oxidation potential after forming an alloy phase with Pd. Due to the effect of hydrogen adsorption on Pd, the specific surface area of the electrochemical activity of the catalyst was calculated by the pre-adsorption monolayer CO dissolution curve (Figure 6). And compared with Pd/C, PdCu/C and PdCuCo/C exhibit a new pair of redox peaks at 0.15 ~ 0.45 V, due to the leaching of exposed Cu atoms from the alloy surface [38]. The standard potential of its alloyed Cu is higher than the Cu/Cu^{2+} standard potential, which indicates that the alloyed Cu in the binary and ternary catalysts are more stable. A Co oxidation peak is not detected in the PdCuCo/C alloy samples, likely because the standard electrode potential of Co ($Co \leftrightarrow Co^{2+} + 2e^-$ is -0.28 V (vs. SCE)) is lower than the potential range applied in the CV measurements. Additionally, the ICP-AES data indicates that the reduction of the Co species was incomplete, which may result in undetected Co oxidation peaks.

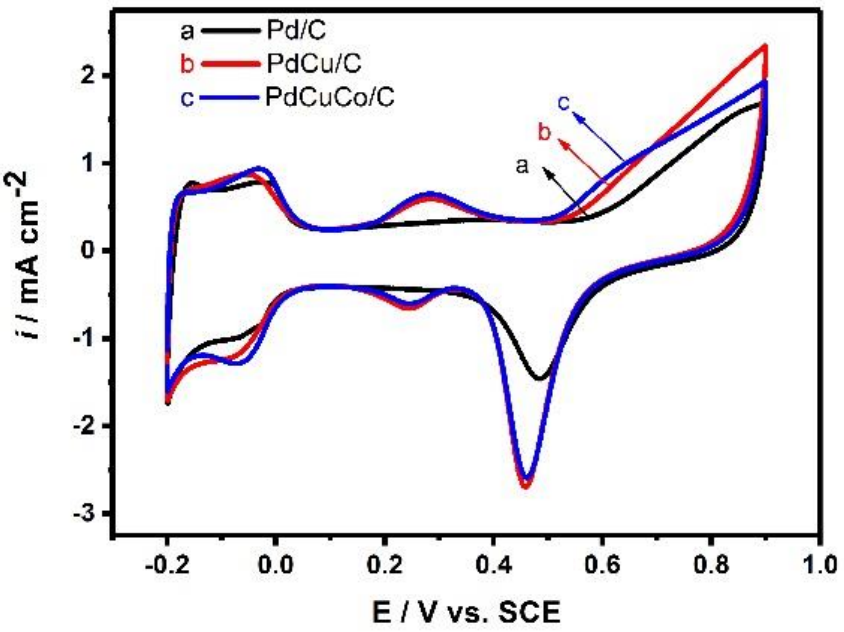

Figure 3. Cyclic voltammograms of Pd/C (a), PdCu/C (b), PdCuCo/C (c) in 0.5 M H_2SO_4 solution at a scan rate of 50 mV s^{-1}.

The electrocatalytic activities of Pd/C (a), PdCu/C (b), and PdCuCo/C (c) catalysts toward the oxidation of formic acid was investigated using linear sweeping voltammetry (LSV) in a 0.5 M H_2SO_4 electrolyte containing 0.5 M HCOOH solution (0.5 M H_2SO_4 / 0.5 M HCOOH) (Figure 4). It can be seen from the Figure 4 that the electrocatalytic oxidation of formic acid is similar for the three catalysts, but the oxidation potential of the PdCu/C, PdCuCo/C catalysts is negatively shifted relative to Pd/C because the adsorption strength of the surface species is weakened after the addition of Cu and Co. The current density for formic acid oxidation (i_p) is in the following order: Pd/C (33.0 mA cm^{-2}) < PdCu/C (50.8 mA cm^{-2}) < PdCuCo/C (60.0 mA cm^{-2}). This suggests the electrocatalysis for formic acid oxidation is significantly increased on PdCu/C and PdCuCo/C. It can be seen that the catalytic current of the PdCuCo/C catalyst for formic acid is the highest and the peak current density of PdCuCo/C is 1.8 times that of the Pd/C catalyst. Furthermore, it can be seen that the PdCuCo/C and PdCu/C catalysts exhibit a lower initial oxidation potential than the Pd/C catalysts, indicating that the addition of the second and third elements reduces the adsorption of species on the catalyst surface. The decrease in the d-band center of Pd further promotes the electrooxidation of formic acid [39]. Table 1 summarizes the comparison of the catalytic efficiency in terms of current density with those of some recently reported Pd-based formic acid electrocatalyst with similar and varying catalyst loadings over GCE. Thus, PdCuCo/C demonstrated excellent potential as a formic acid oxidation reaction anode electrocatalyst, with a lower onset potential, enhanced peak current density, and higher mass acitvity compared to monometallic Pd/C.

Table 1. Comparison of the formic acid oxidation reaction activity for various Pd-based electrocatalysts.

Catalyst	Formic acid Concentration (M)	Electrolyte Concentration (M)	Scan Rate ($mV\ s^{-1}$)	Mass activity ($mA\ mg^{-1}_{Pd}$)	i_p ($mA\ cm^{-2}$)	Ref.
PdCo/C	0.5	0.5 H_2SO_4	50	2467.7	/	[40]
Pd_1Co_1/CNF	0.5	0.5 H_2SO_4	50	/	11.0	[41]
Pd_6Co/3DG	0.5	0.5 H_2SO_4	50	430.8	/	[42]
Pd_1Cu_3/CNTs	0.5	0.5 H_2SO_4	50	560	/	[14]
CuPd/$WO_{2.72}$	0.1	0.1 $HClO_4$	50	2086	/	[43]
PdCu@Pd	0.5	0.5 H_2SO_4	50	501.8	4.93	[44]
Pd_1Cu_1/GN	0.5	0.5 H_2SO_4	50	1390	/	[12]
PdAgNi/C	1	0.5 H_2SO_4	50	428.3	1.6	[45]
PdNiCu/C	0.5	0.5 H_2SO_4	20	792	3.3	[8]
PdCuCo/C	**0.5**	**0.5 H_2SO_4**	**50**	**2142.9**	**60.0**	**This study**

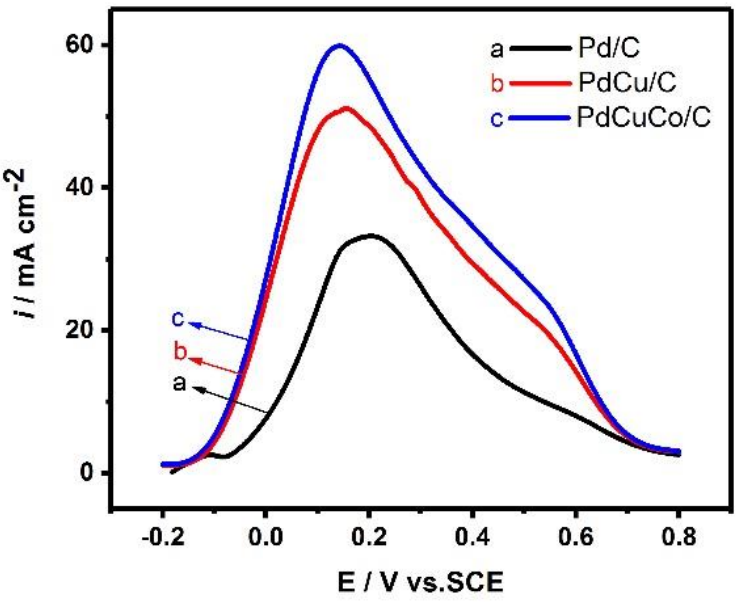

Figure 4. Linear sweeping voltammograms of Pd/C (a), PdCu/C (b), PdCuCo/C (c) in 0.5 M H_2SO_4 / 0.5 M HCOOH at a scan rate of 50 $mV\ s^{-1}$.

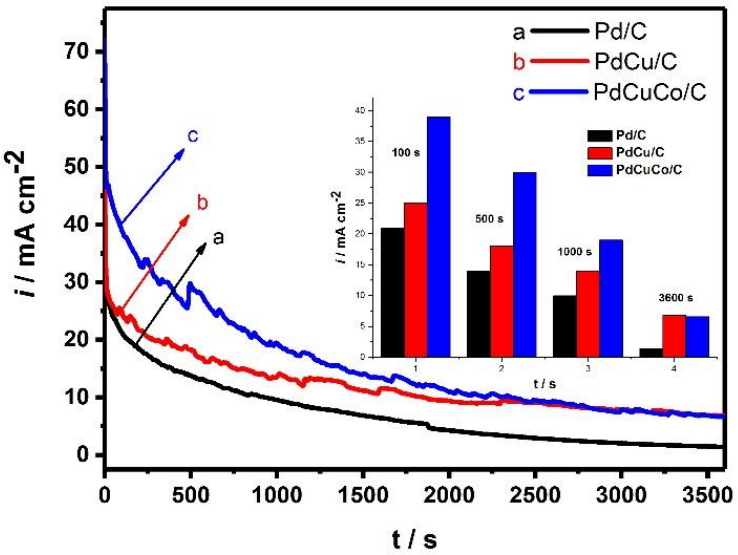

Figure 5. Chronoamperometry curves of Pd/C (a), PdCu/C (b), PdCuCo/C (c) in 0.5 M H_2SO_4 / 0.5 M HCOOH solution at potential of 0.2 V (vs. SCE); the inset is the current densities of formic acid oxidation at 100, 500, 1000, and 3600 s.

Chronoamperometry (CA) of the Pd/C (a), PdCu/C (b), and PdCuCo/C (c) catalysts were conducted at a potential of 0.2 V for 3600 s in a 0.5 M H_2SO_4 / 0.5 M HCOOH solution at a sweep rate of 50 mV s^{-1} to evaluate the electrocatalytic activity and stability (shown in Figure 5). The current densities of formic acid oxidation at 100, 500, 1000, and 3600 s are illustrated in Figure 5. The current density of PdCuCo/C catalyst is 39.1 mA cm^{-2}, 29.9 mA cm^{-2}, 19.3 mA cm^{-2} at 100, 500, 1000 s, respectively. It is apparent that the PdCuCo/C catalyst has the highest current density at all times. After 3600 s, the current density of the PdCuCo/C (6.7 mA cm^{-2}) is 6.7 times and 1.05 times as high as Pd/C (1.0 mA cm^{-2}) and PdCu/C (6.6 mA cm^{-2}), respectively. This may be due to the addition of Cu and Co, which modifies the electronic structure of the precious metal, enhancing the synergistic effect between the three elements.

As shown in Figure 6, the CO-stripping experiments of the three catalysts were studied at 10 mV s^{-1} in 0.5 M H_2SO_4 solution to estimate the anti-poisoning ability of the catalysts, and used to determine the electrochemical surface areas (ECSA) of the catalysts. The ECSA value was calculated as follows [46]:

$$\mathrm{ECSA_{co}} = \frac{\mathrm{Q}}{\mathrm{m \cdot C}} = \frac{\mathrm{S / v}}{\mathrm{m \cdot C}} \qquad (1)$$

The calculated values were listed in Table 2, from which it can be seen that the ECSA values of the three catalysts were Pd/C 55.7 m^2 g^{-1}, PdCu/C 68.8 m^2 g^{-1}, PdCuCo/C 99.5 m^2 g^{-1}, respectively, that is, PdCuCo/C and PdCu/C are significantly higher than Pd/C.

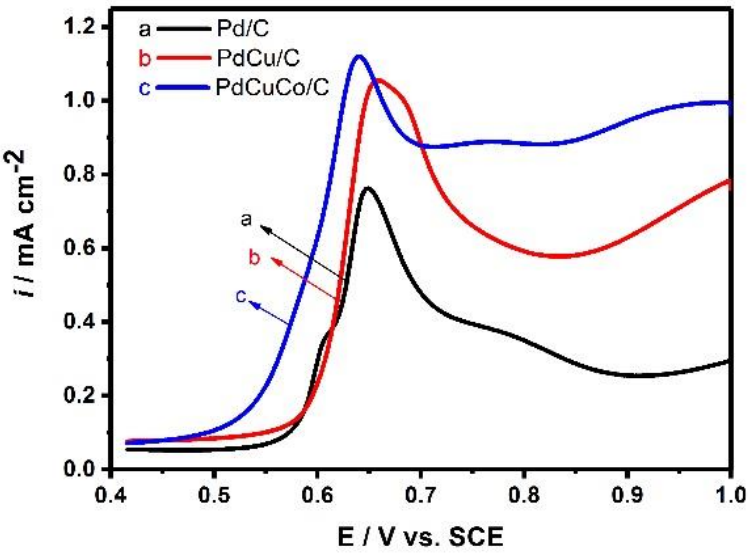

Figure 6. Pre-adsorbed CO-stripping volammograms on Pd/C (a), PdCu/C (b), PdCuCo/C (c) catalysts in 0.5 M H_2SO_4 at a scan rate of 10 mV s^{-1}.

Due to the effect of hydrogen adsorption on Pd, the specific surface area of the electrochemical activity of the catalyst was calculated by the pre-adsorption monolayer CO dissolution curve (Figure 6). It can be seen from Figure 6 that the initial oxidation potential of the PdCu/C and PdCuCo/C catalysts is negatively shifted relative to the Pd/C catalyst. The order, Pd/C (0.56 V) > PdCu/C (0.53 V) > PdCuCo/C (0.49 V), also shows that the stronger the CO oxidation ability, the easier it is to desorb from the metal surface. Therefore, adding Cu and Co increases the electrochemical active area of the catalyst, which provides more reactive sites for the electro-oxidation of formic acid. This may be due to the formation of the alloy phase catalyst. Additional features, including the enhanced synergy between the elements, the manner in which Pd exposes more active area, the enhanced catalyst synthesis method, the small catalyst particle size, and the good dispersion which improves the ECSA [47-48], are all conducive to the electrooxidation of formic acid.

Table 2. Electrochemical characterization for Pd/C, PdCu/C, PdCuCo/C.

Catalyst	ECSA (m^2 g^{-1})	i_p (mA cm^{-2})	E_{onset} of CO stripping (V)	i_{3600}(mA cm^{-2})
Pd/C	55.7	33.0	0.56	1.0
PdCu/C	68.8	50.8	0.53	6.6
PdCuCo/C	99.5	60.0	0.49	6.7

4. CONCLUSIONS

PdCuCo/C nanoalloy catalysts toward formic acid oxidation have been synthesized via a facile one-pot liquid phase chemical reduction method. This preparation method is not only simple, but it also greatly reduces the cost of raw materials. The novel synthesized ternary catalyst features a small particle size, alloying, and good dispersibility on a carbon support. This indicates that the PdCuCo/C catalyst exhibits higher formic acid oxidation performance, higher stability, and better CO poisoning resistance. These features make the material promising for use as a catalyst in direct formic acid fuel cells or other catalytic applications in the liquid fuel cells field.

ACKNOWLEDGEMENTS
This study was funded by the National Science Foundation of China (grant number 21103107) and the Key Project of Shanghai Committee of Science and Technology, China (15DZ1206902).

References

1. N. Cheng, H. Lv, W. Wang, S. Mu, M. Pan, M. Frank, *J. Power Sources*, 195(2010) 7246.
2. X. Wang, J.M. Hu, I. Hsing, *J. Electroanal. Chem.*, 562 (2004) 73.
3. G.L. Soloveichik, *Beilstein J. Nanotech.*, 5 (2014) 1399.
4. X. Yu, P.G. Pickup *J. Power Sources*, 182 (2008) 124.
5. C. Rice, S. Ha, R.I. Masel, A. Wieckowski, *J. Power Sources*, 115 (2003) 229.
6. P.J. Kulesza, I.S. Pieta, I.A. Rutkowska, A. Wadas, D. Marks, K. Klak, L. Stobinski, J.A. Cox, *Electrochim. Acta*, 110 (2013) 474.
7. Z. Liu, L. Hong, M.P. Tham, T.H. Lim, H. Jiang, *J. Power Sources.*, 161 (2006) 831.
8. S. Hu, F. Munoz, J. Noborikawa, J. Haan, L. Scudiero, S. Ha, *Appl. Catal. B-Environ.*, 180 (2016) 758.
9. Y. Wang, F.F. Shi, Y.Y. Yang, W.B. Cai, *J. Power Sources.*, 243 (2013) 369.
10. Z. Gu, Z. Xiong, F. Ren, S. Li, H. Xu, *J. Taiwan Inst. Chem. E.*, 83 (2017) 32.
11. B. Yan, H. Xu, K. Zhang, S. Li, J. Wang, Y. Shi, Y. Du, *Appl. Surf. Sci.*, 434 (2018) 701.
12. S. Li, Y. Zhai, X. Zhang, D.R. Macfarlane, *Adv. Mater, Interfaces*, 4 (2017) 1700227.
13. H. Xu, B. Yan, K. Zhang, J. Wang, S. Li, C. Wang, Y. Du, P. Yang, *Electrochim. Acta*, 261 (2018) 521.
14. Q. Zhao, J. Wang, X. Huang, Y. Yao, W. Zhang, L. Shao, *Electrochem. Commun.*, 69 (2016) 55.
15. F. Yang, Y. Zhang, P.F. Liu, Y. Cui, X.R. Ge, Q.S. Jing, *Int. J. Hydrogen Energy*, 41 (2016) 6773.
16. S. Han, G.S. Chae, J.S. Lee, *Korean J. Chem. Eng.*, 33 (2016) 1799.
17. X. Zhang, *Int. J. Hydrogen Energy*, 13 (2018) 1813.
18. Y. Tang, Y. Chen, P. Zhou, Y. Zhou, L. Lu, J. Bao, T. Lu, *J. Solid State Electr.*, 14 (2010) 2077.
19. G. Sheng, J. Chen, H. Ye, Z. Hu, X.Z. Fu, R. Sun, W. Huang, C.P. Wong, *J. Colloid Interf. Sci.*, 522 (2018) 264.
20. W. Ye, X. Shi, Y. Zhang, C. Hong, C. Wang, W.M. Budzianowski, D.Xue, *ACS Appl. Mater. Inter.*, 8 (2016) 2994.
21. T. Szumełda, A. Drelinkiewicz, E. Lalik, R. Kosydar, D. Duraczyńska, J. Gurgul, *Appl. Catal. B-Environ.*, 221 (2017) 393.
22. S.R. Chowdhury, S. Ghosh, S.K. Bhattachrya, *Electrochim. Acta*, 2017, 225 (2017) 310.
23. N. Cai, C. Jin, C. Wan, R. Dong, *J. Electrochem. Soc.*, 164 (2017) H437.
24. I.M.A. Mohamed, A.S. Yasin, N.A.M. Barakat, S.A. Song, H.E. Lee, S.S. Kim, *Appl. Surf. Sci.*, 435 (2018) 122.
25. M. Li, R. Liu, G. Han, Y. Tian, Y. Chang, *Chinese J. Chem.*, 35 (2017) 1405.

26. L. Wang, J.J. Zhai, K. Jiang, J.Q. Wang, W.B. Cai, *Int. J. Hydrogen Energy*, 40 (2015) 1726.
27. J. Xia, Y. Fu, G. He, X. Sun, X Wang *Mater. Chem. Phys.*, 209 (2018) 86.
28. A.S. Douk, H. Saravani, M. Noroozifar, *J. Alloy Compd.*, 739 (2017) 882.
29. K. Jiang, W.B. Cai, *Appl. Catal. B-Environ.*, 147 (2014) 185.
30. X. Shi, Y. Wen, X. Guo, Y. Pan, Y. Ji, Y. Ying, H.F. Yang, *ACS Appl. Mater. Inter.*, 9 (2017) 25995.
31. J.W. Zhang, B. Zhang, X. Zhang, *J. Solid State Electr.*, 21 (2016) 1.
32. H. Rostami, *Int. J. Hydrogen Energ.*, 42 (2017) 24713.
33. X. Zhang, Y.C. Zhang, J.W. Zhang, B. Zhang, *RSC Adv.*, 5 (2015) 101563.
34. Y. Huang, Y. Guo, Y. Wang, *J. Power Sources*, 249 (2014) 9.
35. F. Liao, T.W.B. Lo, S.C.E. Tsang, *Cheminform*, 7 (2015) 1998.
36. B.R. Cuenya, *Thin Solid Films*, 518 (2010) 3127.
37. W. Pan, X. Zhang, H. Ma, J. Zhang, *J. Phys. Chem. C.*, 112 (2008) 2456.
38. C. Xu, Y. Zhang, L. Wang, L. Xu, X. Bian, H. Ma, Y. Ding, *Chem. Mater.*, 21 (2009) 3110.
39. H.X. Zhang, C, Wang, J.Y. Wang, J.J. Zhai, W.B. Cai, *J. Phys. Chem. C.*, 114 (2010) 6446.
40. Y. Ma, T. Li, H. Chen, X. Chen, S. Deng, L. Xu, D. Sun, Y. Tang, *J. Energy Chem.*, 6 (2017) 1238.
41. D. Liu, Q. Guo, H. Hou, O. Niwa, T. You, *ACS Catal.*, 4 (2014) 1825.
42. L.Y. Zhang, Z.L, Zhao, W. Yuan, C.M. Li, *Nanoscale*, 8 (2016) 1905.
43. Z. Xi, J. Li, D. Su, M. Muzzio, C. Yu, Q. Li, S. Sun, *J. Am. Chem. Soc.*, 139 (2017) 15191.
44. Y. Chen, Y. Yang, G. Fu, L. Xu, D. Sun, J.M. Lee, Y, Tang, *J. Mater. Chem. A,* 6 (2018) 10632.
45. B. Ulas, A. Caglar, O. Sahin, H. Kivrak, *J. Colloid Interf. Sci.*, 532 (2018), 47–57.
46. Y. Yang, Y.H. Li, Y.F. Zhao, P.W. Li, Q.X. Li, *J. Nanopart. Res.*, 20 (2018) 12.
47. L.L. Wang, X.L. Cao, Y.J. Wang, Q.X. Li, *Catalysts*, 5 (2015) 1388.
48. B. Lesiak, M. Mazurkiewicz, A. Malolepszy, L. Stobinski, B. Mierzwa, A. Mikolajczuk-Zychoraa, K. Juchniewicza, A. Borodzinskia, J. Zemekc, P. Jiricekc, *Appl. Surf. Sci.*, 387 (2016) 929.